

RESEARCH

Open Access



AAV-DJ is superior to AAV9 for targeting brain and spinal cord, and de-targeting liver across multiple delivery routes in mice

Monika Chauhan¹, Audrey L. Daugherty¹, Fatemeh (Ellie) Khadir¹, Ozgun F. Duzenli², Alexandra Hoffman³, Jennifer A. Tinklenberg¹, Peter B. Kang¹, George Aslanidi² and Christina A. Pacak^{1*} 

Abstract

Highly efficient adeno associated viruses (AAVs) targeting the central nervous system (CNS) are needed to deliver safe and effective therapies for inherited neurological disorders. The goal of this study was to compare the organ-specific transduction efficiencies of two AAV capsids across three different delivery routes. We compared AAV9-CBA-*fLucYFP* to AAV-DJ-CBA-*fLucYFP* using the following delivery routes in mice: intracerebroventricular (ICV) 1×10^{12} vg/kg, intrathecal (IT) 1×10^{12} vg/kg, and intravenous (IV) 1×10^{13} vg/kg body weight. Our evaluations revealed that following ICV and IT administrations, AAV-DJ demonstrated significantly increased vector genome (vg) uptake throughout the CNS as compared to AAV9. Through the IV route, AAV9 demonstrated significantly increased vg uptake in the CNS. However, significantly fewer vgs were detected in the off-target organs (kidney and liver) following administration of AAV-DJ using the IT and IV delivery routes as compared to AAV9. Distributions of vgs correlate well with transgene transcript levels, luciferase enzyme activities, and immunofluorescence detection of YFP. Overall, between the two vectors, AAV-DJ resulted in better targeting and expression in CNS tissues paired with de-targeting and reduced expression in liver and kidneys. Our findings support further examination of AAV-DJ as a gene therapy capsid for the treatment of neurological disorders.

Keywords AAV capsids, AAV9, AAV-DJ, Gene therapy, Intravenous, Intrathecal, Intracerebroventricular, Neurological, Brain, Spinal cord

Introduction

More than 430 gene therapy trials currently listed on clinicaltrials.gov (<https://clinicaltrials.gov/search?term=%E2%80%9Cgene%20therapy&viewType=Table&cond=Central%20Nervous%20System%20Diseases&locStr=United%20States&country=United%20States> accessed on July 16, 2024) are underway in the United States to investigate a wide variety of gene delivery vehicles for both gene replacement and genome editing therapeutic strategies. The gene therapy field has made significant advancements over the last few decades as there are now Food and Drug Administration (FDA)

*Correspondence:

Christina A. Pacak
cpacak@umn.edu

¹Department of Neurology, Greg Marzolf Jr. Muscular Dystrophy Center, University of Minnesota Medical School, 420 Delaware Street SE, MMC 295, Minneapolis, Minnesota, MN 55455, USA

²The Hormel Institute, University of Minnesota, Austin, MN, USA

³University of Maryland, Baltimore, MD, USA



© The Author(s) 2024. **Open Access** This article is licensed under a Creative Commons Attribution 4.0 International License, which permits use, sharing, adaptation, distribution and reproduction in any medium or format, as long as you give appropriate credit to the original author(s) and the source, provide a link to the Creative Commons licence, and indicate if changes were made. The images or other third party material in this article are included in the article's Creative Commons licence, unless indicated otherwise in a credit line to the material. If material is not included in the article's Creative Commons licence and your intended use is not permitted by statutory regulation or exceeds the permitted use, you will need to obtain permission directly from the copyright holder. To view a copy of this licence, visit <http://creativecommons.org/licenses/by/4.0/>.

approved therapies for multiple genetically inherited disorders that were once considered untreatable [1–9].

Adeno-associated virus (AAV) is one of the most efficient vehicles available to deliver healthy gene cDNA sequences into the cells of affected individuals due to its ability to persist for long periods of time as an episome within the nuclei of cells, its relatively non-pathogenic nature, and its ability to infect dividing and non-dividing cells in vivo [10, 11]. Despite these advantages, one key challenge related to the use of AAV includes the high doses currently required to achieve a sufficient therapeutic effect. High doses of intravenously administered AAV can elicit responses in both the innate and adaptive immune systems [12–14]. There are both vector-dependent and host-dependent factors that influence the immunogenicity of AAV capsids and subsequent severity of immune responses [14, 15]. Major obstacles related to immune responses include the presence of host neutralizing antibodies against AAV [16] and the activation of CD4⁺ and CD8⁺ T cells in response to degradation of either capsid or transgene-encoded proteins by the proteasome [17]. These inflammatory responses can be further amplified by activation of the alternative complement pathway through direct interactions between complement component C3 and AAV capsid proteins [12]. Efforts to reduce the therapeutic dose to help increase safety, reduce immune responses, and improve the therapeutic efficacy of gene therapies promise to yield significant clinical benefits. One approach to improve AAV-based therapeutics is to develop synthetic capsid serotypes, such as AAV-DJ, that are optimal for transducing desired organs and cell types while simultaneously avoiding off-target organs and evading immune responses. Another approach to target desired regions is to perform AAV administrations through different delivery routes, such as intrathecal (IT) delivery to further improve CNS targeting [18, 19].

Our interest in the development of AAV-mediated gene-based therapies for rare neurological disorders led us to explore novel capsids for targeting specific regions and cells within the brain and spinal cord. Genetic disorders associated with neurological pathologies are particularly difficult to treat. This is in part due to challenges associated with the penetration of the highly protective blood-brain barrier (BBB) and central nervous system (CNS) complexities that can result in limited access to the brain's deep structures. Unique AAV capsid motifs for each serotype are critical for binding to host cells and represent a key step in the specificity of AAV-mediated gene delivery. We thus compared the AAV9 capsid currently used in the FDA approved gene therapy for spinal muscular atrophy (SMA) (onasemnogene abeparvovec-xioi) to the AAV-DJ synthetic capsid that was developed by shuffling naturally occurring serotypes [20]. AAV-DJ

was recently demonstrated to be superior for the broad transduction of neurological tissue in a non-human primate study [21] and was originally selected in part, due to the lower prevalence of neutralizing AAV-DJ antibodies in humans [20].

Another important consideration is the gene therapy delivery route. Therefore, we also compared the efficiency of AAV9 and AAV-DJ capsids across three different delivery routes with respect to their ability to target the CNS and simultaneously de-target the liver and kidney. We are particularly keen to avoid the liver as AAVs that are delivered systemically tend to be sequestered in the liver [22, 23]. This leads to reduced transduction of target (non-liver) organs and potentially liver toxicity [24, 25], which may in some cases be fatal [26]. Our study will help optimize capsid selection and delivery route for CNS gene therapies.

Materials and methods

AAV production and purification

Both AAV9 and AAV-DJ vectors were packaged in a single-strain expression cassette with chicken β -actin (CBA) promoter-driven fusion of firefly luciferase (fLuc), and yellow fluorescent protein (YFP) [27, 28]. Recombinant AAV vectors were produced using the triple transfection method and purified as described previously [29, 30]. Briefly, HEK293 cells were co-transfected with three plasmids encoding (1) Rep/Cap, (2) ITRs-CBA-fLuc-YFP, and (3) Ad helper genes using polyethyleneimine (#23966-1, Polysciences, USA). Cells were harvested 72 h post transfection, subjected to freeze-thaw cycles, and treated with Benzonase (#E8263, Sigma-Aldrich, USA) at 37 °C for 1 h. The suspension was purified by Iodixanol (#D1556, Sigma-Aldrich, USA) gradient ultracentrifugation followed by ion exchange chromatography using HiTrap Q HP (Cytiva, USA) with Bis-Tris propane-MgSO₄ buffer. Subsequently, the vector preparation was concentrated into 10 mM Tris – 100 mM sodium citrate buffer (pH 7) using centrifugal spin concentrators (#AP2015010, Orbital Biosciences, USA).

Quantitative PCR analysis for the determination of AAV titers

For vector genome (vg) titer determination, DNA contaminants were removed by TURBO DNase (#REF4022G, Thermo Fisher Scientific, USA) digestion. AAV genomes were then released from AAV capsids by Proteinase K (#AM2546, Invitrogen, USA) digestion. Subsequently, the viral DNA was cleaned using DNA Clean & Concentrator™ 25 (#11-305 C, Genesee Scientific, USA). Vector titers were quantified by qPCR with a TBGreen Advantage (#S4748, Takara Bio, USA), using the following primer pair specific to the CBA promoter region within the viral cassette: forward primer 5'-TCCC

ATAGTAACGCCAATAGG –3' and reverse primer 5'-C TTGGCATATGATACACTTGATG –3' [29, 30].

Animals

All husbandry and procedural use of animals was approved by the Institutional Animal Care and Use Committee (IACUC) at the University of Minnesota (UMN). All the FVB/NJ (stock# 001800) mice (5 weeks old) were ordered from Jackson Laboratory. The mice were maintained at 25 °C and 50% humidity in the Research Animal Resources facility at UMN. Animals were maintained in 14/10 h light/dark cycles and fed chow and water ad libitum. All animals used in the study were acclimatized in the vivarium and handled for one week prior to initiation of the study.

Routes of AAV delivery

Equal numbers of males and females were used for each delivery route and capsid. In total, for every route, 10 (5 males and 5 females) 6-week-old mice were injected with AAV9-CBA-*fLuc/YFP* and 10 (5 males and 5 females) 6-week-old mice were injected with AAV-DJ-CBA-*fLuc/YFP*.

Jugular vein injection (IV)

IV administration was performed as previously described [31, 32]. Briefly, mice were anesthetized with inhaled 1–3% isoflurane (Dechra, USA). A small incision (~0.5 cm) was made parallel to the midline at the lower third of the right anterior neck, exposing the right external jugular vein. A 28-gauge insulin needle was bent on the sterile surface and used to slowly inject 150 µL of AAV-CBA-*fLuc/YFP* or vehicle (1x PBS) into the vein. Gentle pressure was applied on the skin to achieve hemostasis and the incision was closed with the tissue adhesive (Vetbond, 3 M animal care products, USA). 1×10^{13} vg/kg body weight per mouse was injected in a total volume of 150 µL. Meloxicam (OstiLox, VETone, UK) at 0.5 mg/kg was injected subcutaneously as an analgesic for 72 h post-surgery. Animals were monitored carefully post-surgery according to IACUC instructions.

Intrathecal injection (IT)

For intrathecal injections, mice were anesthetized as mentioned above. Hair was removed from a small area on the lower back and scrubbed. A Hamilton syringe (26 gauge) was used to deliver the AAV (1×10^{12} vg/kg body weight per mouse, this dosage was used due to injection volume limitation) directly by lumbar puncture (between the fifth lumbar (L5) and the sixth lumbar (L6) vertebrae) in a total volume of 10 µL [33–36]. Male and female cohorts were injected for both capsids separately as mentioned above.

Intracerebroventricular injection (ICV)

For bilateral ICV injections, mice were anesthetized, hair was removed from the area between the ears, the head was fixed into the stereotaxic apparatus and scrubbed. A small incision was made, a T-shaped subcutaneous junction (bregma) was identified, a 26 gauge Hamilton needle attached to the apparatus was adjusted to that point, and subsequently the apparatus values for dorsoventral axis were set to zero. The needle was directed to the lateral ventricles: –0.5 mm in the anteroposterior axis, ± 1 mm in the mediolateral axis, and –2.3 mm in the dorsoventral axis (~2 months old mouse coordinated according to Allen Brain Atlas). Once the needle was placed inside the ventricle, 5 µL of AAV-CBA-*fLuc/YFP* or vehicle (1x PBS) was injected slowly into the ventricle with a flow rate of 1 µL per minute to enable further diffusion [37]. Before slow withdrawal of the needle, there was a 2 min wait time to ensure complete diffusion of the injected fluid and no back-flow of the delivered virus. The other hemisphere was injected using the same procedure. The total injected AAV dose was 1×10^{12} vg/kg body weight per mouse (this dosage was used due to injection volume limitations using this delivery route in mice). The incision was closed with tissue adhesive (Vetbond, 3 M animal care products, USA), and meloxicam (OstiLox, VETone, UK) at 0.5 mg/kg was injected subcutaneously as an analgesic for 72 h post-surgery. Animals were monitored carefully post-surgery according to IACUC instructions.

In vivo live imaging

Two weeks following AAV administration, in vivo imaging was performed to monitor luciferase expression in live animals. The mice were administered with D-luciferin (#770504, IVISbrite D-LuciferinRediject, PerkinElmer, USA) through intra-peritoneal (IP) injections at a dose of 150 mg/kg of body weight. After 15 min, mice were subjected to anesthesia (isoflurane inhalation) followed by bioluminescence imaging analysis using an in vivo optical imaging system (IVIS100 IVIS® Imaging System, PerkinElmer, USA). Raw images containing raw data were then analyzed in M3Vision software (Living Image Software, PerkinElmer), using the freehand tool to obtain total luciferase signals from each organ. Data were exported in photons (ph)/s/cm²/steradian unit and displayed as a pseudo-color overlay onto the animal image, using a rainbow color scale.

AAV vector genome (vg) determination

AAV vg copy numbers from various mouse tissues were determined as previously described [31, 32] by qPCR after extraction of total genomic DNA (gDNA) using DNeasy Blood and Tissue kit (#69506, Qiagen, Germany). Tissues were mechanically homogenized using a bead basher (BenchMark) with the kit lysis buffer. gDNA

was isolated according to manufacturer instructions. Vg content in each tissue was determined using 100 ng total DNA using the qPCR method on the Applied Biosystems QuantStudio 3 thermal cycler and a Taqman probe specific for the luciferase reporter sequence (Assay ID: Mr03987587_mr, Thermo). Luciferase plasmid DNA dilutions with known copy number were used to create a standard curve to extrapolate absolute copy numbers in the tissue sample gDNA [38, 39].

Transcript analysis

Total RNA was isolated from mouse tissues using the Quick-RNA MiniPrep kit (#R1055, Zymo Research, USA) according to manufacturer's instructions. The RNA kit includes a gDNA removal step. 300 ng of total gDNA-free-RNA was used for cDNA synthesis using the High-Capacity RNA-to-cDNA Kit (#4388950, Applied Biosystems, USA). This cDNA product served as the template for qPCR with luciferase probes (Assay ID: Mr03987587_mr, Thermo, USA) and the Applied Biosystems QuantStudio 3 thermal cycler. Ribosomal RNA 18s amplification (Assay ID: Mm03928990_g1, Thermo, USA) on the same cDNA was used as an internal control. Fold change in luciferase transcripts was calculated using the $\Delta\Delta C_T$ method.

Luciferase assay

The frozen tissues (~25 mg) were homogenized in 400 μ L of 1x reporter lysis buffer (#E1501 kit, Promega), and the lysates underwent 3 freeze thaw cycles (-80°C to 37°C). The samples were centrifuged for 3 min. at 10,000 x g and supernatants were collected for the assay. In a 96 well plate (white bottom) 20 μ L lysate was mixed with 50 μ L Luciferase Assay Reagent (#E1501 kit, Promega) (as per the manufacturer's instructions). The samples were run in triplicates and luminescence was measured with a 10,000ms integration time using the SpectraMax i3x plate reader (Molecular Devices).

Immunohistochemistry

Animals used for immunohistochemistry studies were euthanized by perfusion fixation as previously described [40, 41]. Mice were anaesthetized with isoflurane and perfused with sterile 1x PBS (pH 7.4) followed by a fixative (4% paraformaldehyde (PFA) in 1x PBS). Tissues were removed post fixation and placed in 4% PFA for 12 h overnight. The next day, the tissues were dehydrated and embedded into paraffin blocks. Sections were cut at 7 μ m thickness and mounted onto pre-charged slides (#12-550-15 Superfrost Plus slides, Fisher Scientific, USA). For immuno-fluorescence (IF), tissue sections were rehydrated in 100% xylene, ethanol gradient (100%, 70%, 50%), and then water. Sections were permeabilized for 30 min at room temperature in 1x PBS containing 0.3% Triton

X-100 and then incubated for 1 h in blocking solution (1x PBS containing 3% BSA, 2% normal donkey serum, and 0.15% Triton X-100). The same blocking reagent was used to prepare primary antibody dilutions which were incubated on samples overnight at 4 °C. The primary antibodies used include: mouse monoclonal anti-GFP/YFP 1:50 (#A11121, Invitrogen), (specificity was confirmed by lack of labeling in the vehicle treatment group); rabbit anti-NeuN 1:100 (#26975-I-AP, Proteintech), rabbit anti-GFAP 1:100 (#NB300-141, Novus Biologicals), rabbit anti-OLIG2 1:100 (#13999-1-AP, Proteintech). After a 5-minute 1x PBS rinse, sections were incubated for 1 h at room temperature with appropriate combinations of Alexa Fluor (1:500, AF568 goat anti-rabbit #A11036 and AF488 goat anti-mouse #A11029, Invitrogen) conjugated secondary antibodies (Life Technologies, Invitrogen). Sections were rinsed again in 1x PBS. Following the final rinses, sections were cover-slipped using a mounting solution containing DAPI (#P36962, ProLong Diamond Antifade Mountant, Invitrogen). Tissues from 1x PBS sham-injected mice were processed in parallel with the AAV-CBA-*fLuc/YFP* treated tissues and were included in all immunohistochemical experiments to control for non-specific staining of the YFP antibody.

Microscopy and image analysis

Images were collected on a Leica DM5500 B epi-fluorescent microscope with LAS-X software. For comparisons of tissues from ICV, IT, and IV injected mice, images were collected using the same microscope setting with a few exceptions where adjustments were necessary to allow detection of labeling in IT treated tissues or avoid saturation in ICV and IV treated tissues. Similarly, image adjustments for contrast, brightness, and color were performed in parallel for all delivery routes and treated tissues. For each mouse tissue, 5 non-overlapping images (2 from the cortex region, 2 from the hippocampus region, and 1 from the thalamus region from each brain slice) were taken from each of 3 tissue sections (brain slices). These were then evaluated by a trained, blinded observer. Different cell types in the brain were identified based on visualization with cell-type specific antibodies, and only cells with visible nuclei were counted. Total numbers of YFP positive cells were counted using the cell counter plugin in Image J software. The percentage of YFP positive cells were calculated from the total number of each cell type.

Statistical analysis

The data are expressed as mean or percentage \pm standard error of the mean (SEM) from at least three animals unless indicated otherwise. For in vivo mouse imaging experiments, 8 mice were analyzed (front and back for 16 total data points) per treatment. For vgs, RNA, and

luciferase assays, tissues from 6 mice were used in each group. For all IF studies, tissues from three different animals were analyzed. All the bar graph results are shown as mean \pm SEM. No data were excluded from analyses. For determining the cell type counting with immunofluorescence assay images, the study investigators A.L.D and A.H. were blinded to treatment groups using codes generated by an independent investigator (M.C.). Five male and five female mice were used for each AAV delivery cohort. Comparisons were made using one-way analysis of variance (ANOVA) followed by a Bonferroni post-hoc test or by a two-tailed student t-test unless otherwise indicated. In figure legends, n indicates the number of animals used in the study (biological replicates). P values were calculated by the indicated statistical tests using GraphPad Prism (v.10.4.0) software.

Results

For all in vivo studies to assess the biodistribution of AAV9 and AAV-DJ, we used a ubiquitous Chicken β -actin (CBA) promoter to drive the expression of a firefly luciferase (*fLuc*) fused to a yellow fluorescent protein (YFP). This combination of promoter and transgene allowed for a versatile and highly sensitive evaluation of CNS expression for comparisons of each capsid using the intravenous (IV), intrathecal (IT), and intracerebroventricular (ICV) delivery routes in healthy wild-type FVB/NJ mice. For the ICV and IT routes, each mouse received 1×10^{12} vg/kg of either AAV9-CBA-*fLuc*/YFP, AAV-DJ-CBA-*fLuc*/YFP, or an equivalent volume of 1x PBS (for injection controls). For the IV route, each mouse

received 1×10^{13} vg/kg of either AAV9-CBA-*fLuc*/YFP, AAV-DJ-CBA-*fLuc*/YFP, or an equivalent volume of 1x PBS (Fig. 1A). No difference between males and females was observed in any cohort. Mice from all cohorts were imaged for detection of luciferase mediated bioluminescence at three, seven, and nine weeks post-AAV administration (Fig. 1B).

Bioluminescence was detected from all AAV9 and AAV-DJ treated mice throughout every imaging session. As our goal was to primarily target the CNS, head/body radiance ratios were determined to provide relative bio-distribution of expression information. Mice from both the ICV and IT AAV-DJ cohorts displayed a significant increase in relative head/body ratios at nine weeks as compared to those treated with AAV9 using the same delivery routes (Fig. 2A-D, Supp. Figure 1). In comparison, mice from the IV delivery route that were administered AAV9 displayed significantly higher head/body ratios at nine weeks as compared to those in the AAV-DJ cohort (Fig. 2F).

To quantify both the efficiency of gene transfer to various regions of the CNS and de-targeting of liver and kidney, full necropsies were performed on six mice from each cohort at nine weeks post-AAV administration. gDNA was isolated and AAV vector genome (vg) bio-distribution was determined across the following brain regions: hippocampus, hypothalamus, cerebellum, and cortex, as well as spinal cord, liver, and kidney (Fig. 3). Using the IT and ICV routes, vg levels in the AAV-DJ cohorts were significantly higher than those from AAV9 cohorts in the hippocampus, hypothalamus, cerebellum,

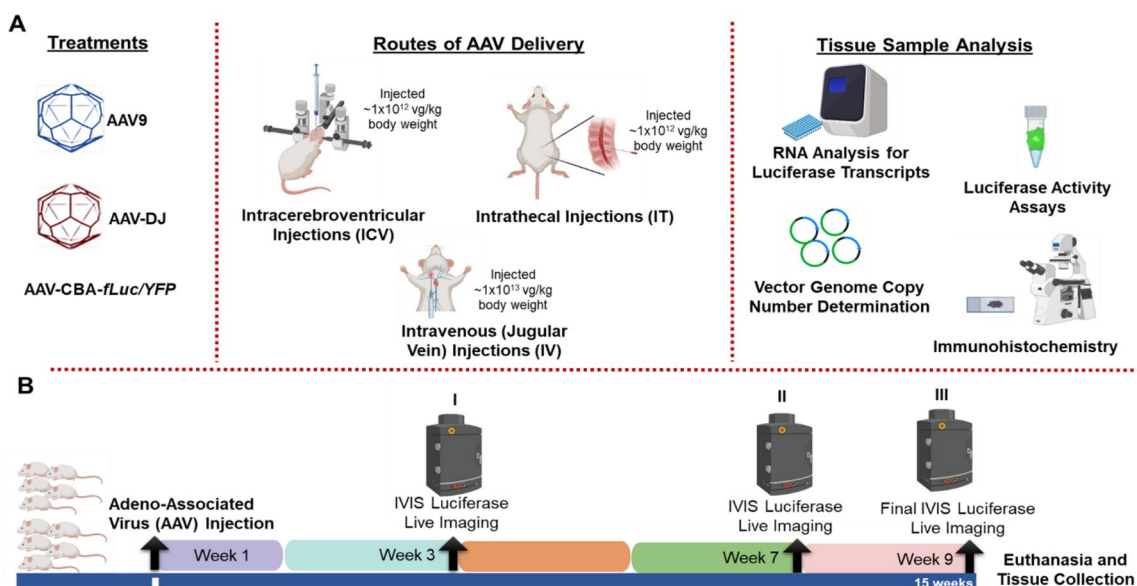


Fig. 1 Experimental overview of capsid and delivery route comparisons. **(A)** WT FVB/NJ mice at ~ 6 weeks of age were injected via intracerebroventricular (ICV), intrathecal (IT), or jugular vein (IV) injections with AAV9 or AAV-DJ to deliver a luciferase - yellow fluorescent protein (YFP) fusion protein. **(B)** Mice were evaluated throughout the study through non-invasive luciferase live imaging at the end of weeks 3 (I), 7 (II) and 9 (III). Nine weeks after AAV delivery, six mice (3 males and 3 females) were euthanized for DNA, RNA, and protein analysis and four mice (2 males and 2 females) for histological studies

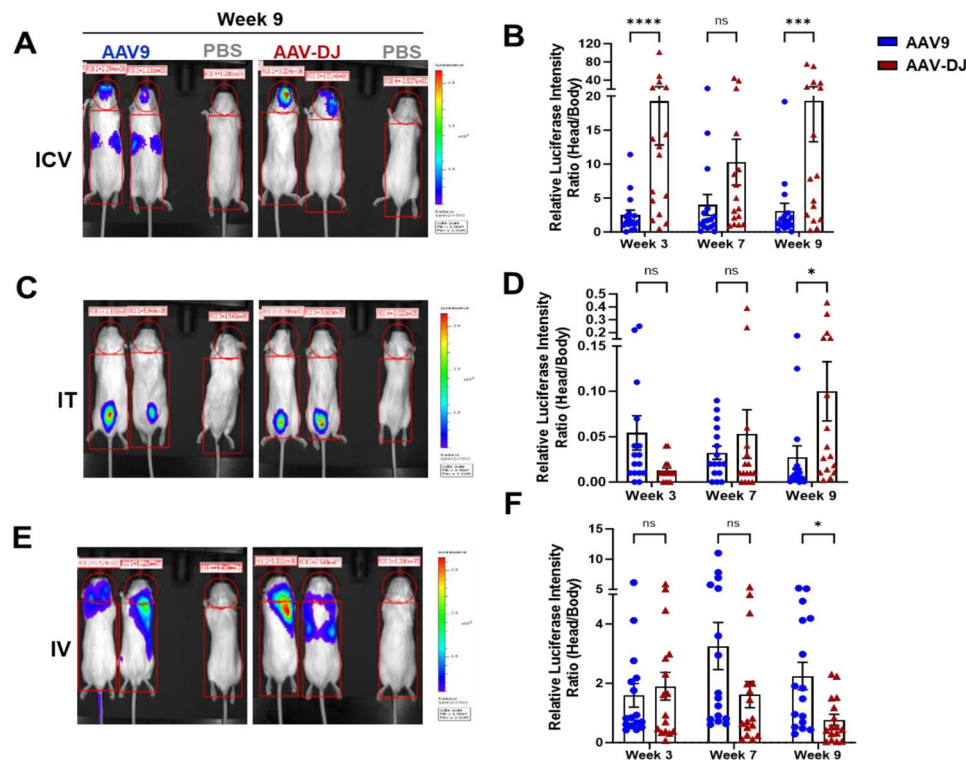


Fig. 2 Visualization and quantification of differential Luciferase expression patterns using IVIS whole-body live bioluminescence imaging in WT FVB/NJ mice. 1×10^{12} vg/kg (ICV or IT) or 1×10^{13} vg/kg (IV) of AAV (AAV-CBA-*fluc*/*YFP*) encoding the luciferase transgene was delivered into 6 week old mice via (A) ICV, (C) IT, or (E) IV administrations. Luciferase expression levels were detected by injecting luciferin substrate 15 min prior to bioluminescence imaging at 3, 7, and 9 weeks after vector administrations. Representative images of two mice from the AAV9 and AAV-DJ groups for Week 9 (post AAV delivery) are shown. Mouse 1 located on the right side of each image is the no virus control. Luciferase intensities from both the dorsal and ventral sides of each animal were obtained and head to body ratios were calculated and presented in the graphs (B) ICV, (D) IT and (F) IV. There are 16 data points from a total of 8 mice per cohort. The data are displayed as mean values \pm SEM ($N=8$ mice per group; * $p < 0.05$, **** $p < 0.001$, ns- not significant based upon unpaired two-tailed t-tests)

cortex, and spinal cord (Fig. 3A-E). In contrast, IT administration of AAV9 resulted in significantly higher levels of vgs in the off-target liver and kidney while ICV administration showed no differences between the two capsids (Fig. 3F, G). Using the IV delivery route, mice in the AAV9 cohort displayed significantly higher vg levels in the hypothalamus, cerebellum, and cortex as well as in the off-target organs liver and kidney as compared to AAV-DJ. IV delivery with the AAV-DJ capsid resulted in significantly higher vg levels in the hippocampus and spinal cord as compared to AAV9.

To further examine the efficiency of gene delivery by AAV-DJ and AAV9, luciferase gene transcription levels were assessed in the CNS and off-target organs. Total RNA was isolated from each tissue and luciferase transcription levels were assessed by quantitative PCR. The hippocampus, cerebellum, cortex, and spinal cord from the IT groups demonstrated significantly higher transcription levels following delivery with AAV-DJ whereas the hypothalamus, liver, and kidney had higher levels following delivery with AAV9 (Fig. 4A-G). The hippocampus, hypothalamus, cerebellum, spinal cord, and cortex

from the ICV group all demonstrated significantly higher transcription levels following delivery with AAV-DJ whereas the liver and kidney showed no significant differences in expression levels between AAV-DJ and AAV9. Every neurological tissue analyzed except the cerebellum showed significantly higher expression following the use of IV administered AAV9 (Fig. 4A-E). However, both off-target organs (liver and kidney) also showed significantly higher expression levels with AAV9 (Fig. 4F, G).

Luciferase activity assays were used to quantify relative luciferase protein levels among organs and cohorts. Relative light units (RLUs) were normalized to the amount of total protein for each respective sample. The hippocampus, cerebellum, cortex, and spinal cord from the IT groups demonstrated significantly higher luciferase activity levels following delivery with AAV-DJ whereas the hypothalamus, liver, and kidney had higher levels following delivery with AAV9 (Fig. 5A-G). The hippocampus, hypothalamus, cerebellum, cortex, and spinal cord from the ICV group all demonstrated significantly higher luciferase activity levels following delivery with AAV-DJ, whereas the liver showed higher levels with AAV9 and

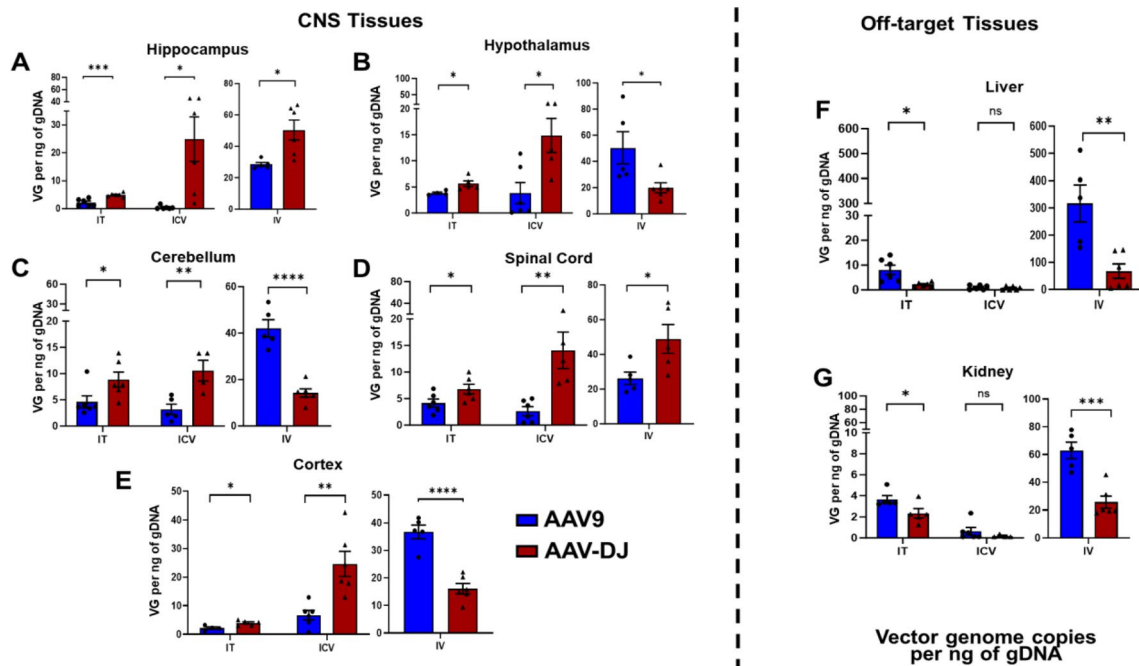


Fig. 3 AAV vector genome (vg) estimations in tissues of interest. gDNA was isolated and luciferase transgene vg numbers were calculated per ng of gDNA for (A-E) neurological tissues (hippocampus, hypothalamus, cortex, cerebellum, spinal cord) and off-target tissues F) liver and G) kidney. Data are presented as mean ± SEM of the values from six mice (* $p < 0.05$, ** $p < 0.01$, *** $p < 0.001$, ns- not significant based upon unpaired two-tailed t-tests)

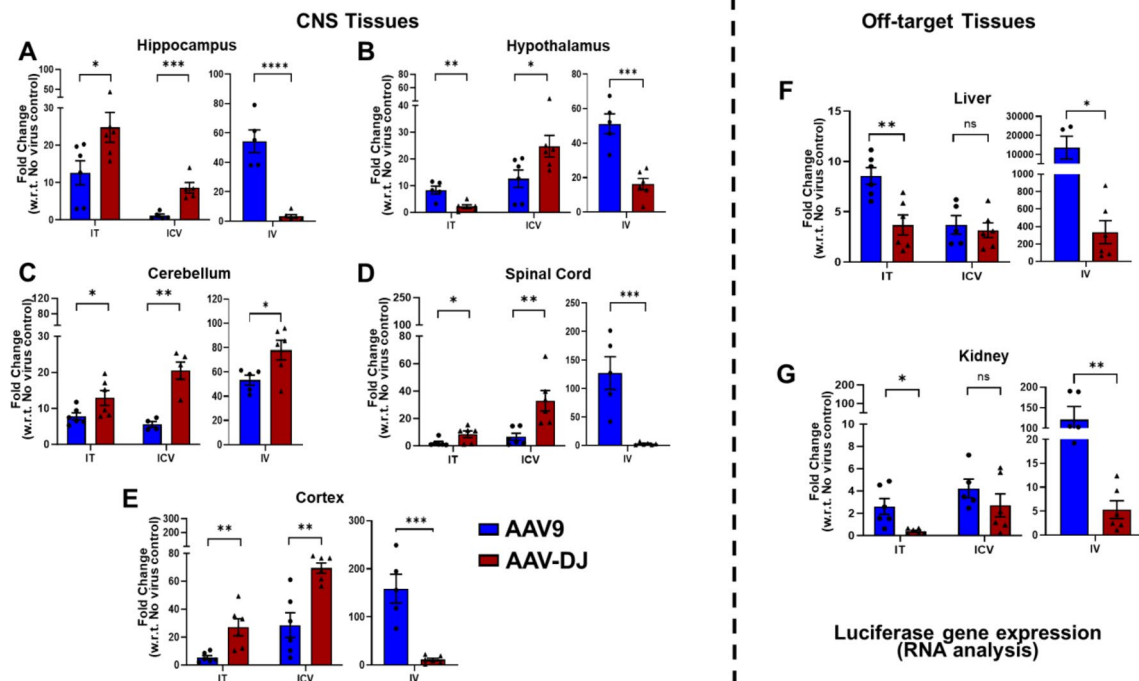


Fig. 4 Luciferase transgene transcript levels in tissues of interest. Total RNA was isolated, converted to cDNA, and fold changes in luciferase mRNA transcript expression levels were calculated as compared to no virus controls for (A-E) neurological tissues (hippocampus, hypothalamus, cortex, cerebellum, spinal cord) and off-target tissues F) liver and G) kidney. Data are presented as mean ± SEM of the values from six mice (* $p < 0.05$, ** $p < 0.01$, *** $p < 0.001$, ns- not significant based upon unpaired two-tailed t-tests)

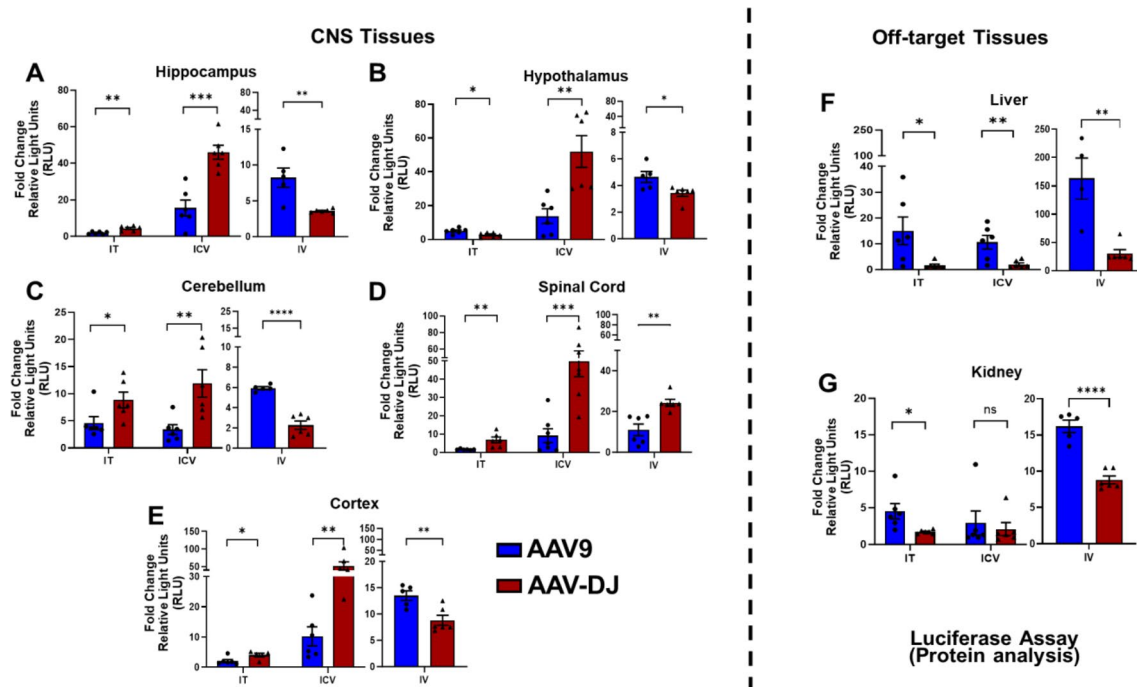


Fig. 5 Luciferase activity assays in tissues of interest. Relative luciferase activities were measured and normalized to total protein concentrations and presented as fold changes in relative light units (RLUs) were calculated as compared to no virus controls for (A-E) neurological tissues (hippocampus, hypothalamus, cortex, cerebellum, spinal cord) and off-target tissues (F) liver and (G) kidney. Data are presented as mean \pm SEM of the values from six mice ($*p < 0.05$, $**p < 0.01$, $***p < 0.001$, $****p < 0.0001$, ns- not significant based upon unpaired two-tailed t-tests)

the kidney showed no significant differences in expression levels between AAV-DJ and AAV9 (Fig. 5A-G). Every neurological tissue analyzed except the spinal cord showed significantly higher activity levels following the use of IV administered AAV9 (Fig. 5A-E). Both off-target organs (liver and kidney) also showed significantly higher levels with AAV9 (Fig. 5F, G).

Immunofluorescence (IF) staining was performed to identify differences in the ability of AAV9 and AAV-DJ to transduce specific neurological cell types. Co-immunostaining to detect YFP transgene expression and molecular markers for neurons (neuronal nuclei, NeuN), oligodendrocytes (olig2), and astrocytes (glial fibrillary acidic protein, GFAP) was performed on fixed brain slices from three mice representing each cohort. To facilitate quantitative evaluations of gene transfer efficacies between cohorts, the numbers of YFP/NeuN, YFP/olig2, and YFP/GFAP double-positive cells among the total number of neurons, oligodendrocytes, or astrocytes (respectively) were determined following imaging of coronal mouse brain sections (Supp. Figures 2, 3, 4, and 5).

Both the AAV9-CBA-*fLuc*/YFP and AAV-DJ-CBA-*fLuc*/YFP vectors yielded a similar general distribution of expression in neurons across brain regions (Supp. Figure 3 and Fig. 6). Following ICV administrations, YFP expression was detected in $5.32\% \pm 3.98\%$ (AAV9) and $11.77\% \pm 8.93\%$ (AAV-DJ) of NeuN+ cells (Fig. 6A). Following IT administrations, YFP expression was detected

in $5.07\% \pm 2.83\%$ (AAV9) and $6.50\% \pm 5.60\%$ (AAV-DJ) of NeuN+ cells (Fig. 6B). Following IV administrations, YFP expression was detected in $8.43\% \pm 3.21\%$ (AAV9) and $5.46\% \pm 2.16\%$ (AAV-DJ) of NeuN+ cells (Fig. 6C).

Both the AAV9-CBA-*fLuc*/YFP and AAV-DJ-CBA-*fLuc*/YFP vectors yielded a similar general distribution of expression in oligodendrocytes across brain regions (Supp. Figure 4 and Fig. 7). Following ICV administrations, YFP expression was detected in $12.19\% \pm 7.18\%$ (AAV9) and $19.61\% \pm 7.88\%$ (AAV-DJ) of olig2+ cells (Fig. 7A). Following IT administrations, YFP expression was detected in $16.45\% \pm 9.01\%$ (AAV9) and $14.32\% \pm 5.48\%$ (AAV-DJ) of olig2+ cells (Fig. 7B). Following IV administrations, YFP expression was detected in $16.82\% \pm 10.49\%$ (AAV9) and $9.92\% \pm 5.13\%$ (AAV-DJ) of olig2+ cells (Fig. 7C).

Both the AAV9-CBA-*fLuc*/YFP and AAV-DJ-CBA-*fLuc*/YFP vectors yielded a similar general distribution of expression in astrocytes across brain regions (Supp. Figure 5 and Fig. 8). Following ICV administrations, YFP expression was detected in $14.15\% \pm 4.28\%$ (AAV9) and $17.49\% \pm 4.97\%$ (AAV-DJ) of GFAP+ cells (Fig. 8A). Following IT administrations, YFP expression was detected in $14.46\% \pm 6.13\%$ (AAV9) and $15.89\% \pm 5.84\%$ (AAV-DJ) of GFAP+ cells (Fig. 8B). Following IV administrations, YFP expression was detected in $12.28\% \pm 5.40\%$ (AAV9) and $16.92\% \pm 6.93\%$ (AAV-DJ) of GFAP+ cells (Fig. 8C).

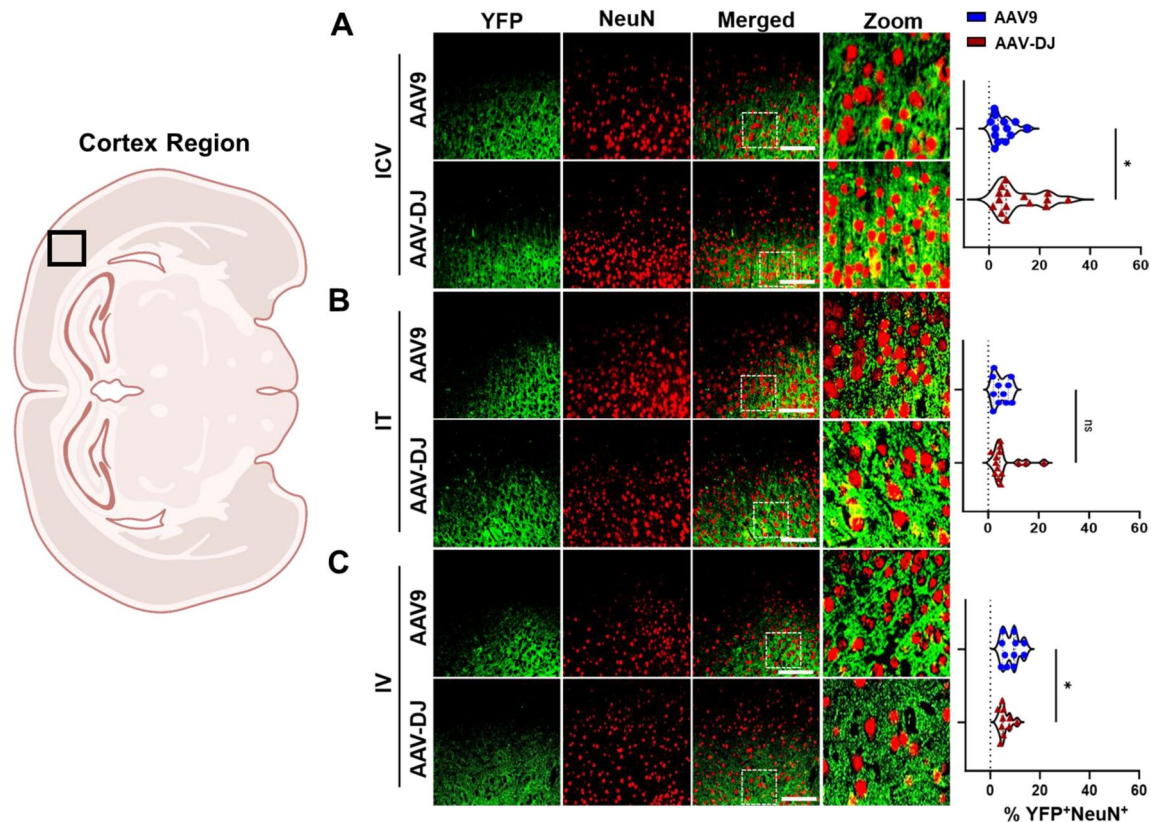


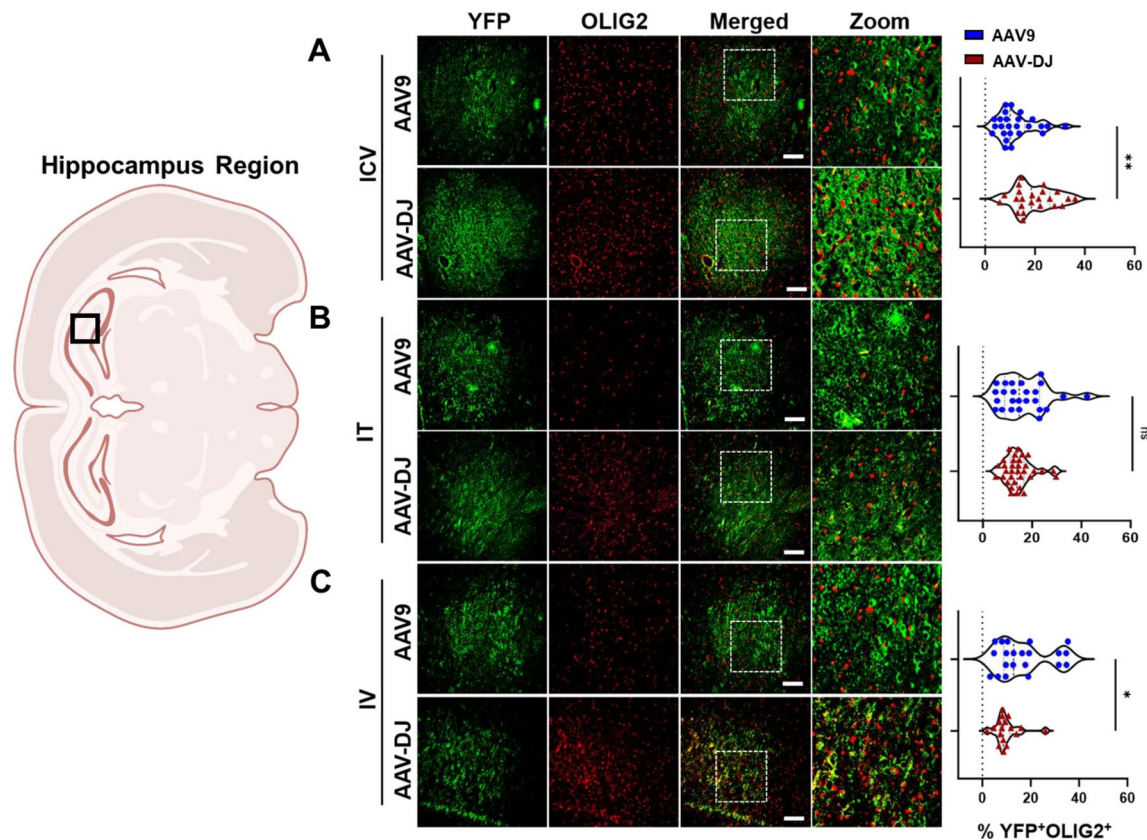
Fig. 6 Relative transduction of neurons between cohorts. YFP transgene expression was compared to a neuronal cell marker (NeuN) and co-localization was quantified across cohorts through blinded analysis. Representative immunofluorescence images (from the cortex region as indicated in the brain overview image on the left) from each cohort (**A**) ICV, (**B**) IT, and (**C**) IV are provided. For each mouse tissue, five non-overlapping images were acquired from across each of three tissue sections, and evaluated by a trained, blinded observer. The percentages of YFP⁺/NeuN⁺ cells are presented in the right-hand panels. Scale bars = 100 μ m. The white box indicates the zoomed-in portion of the image that is displayed to the right of each row of images

Based upon these data, the AAV-DJ capsid transduces significantly more neurons, astrocytes, and oligodendrocytes than the AAV9 capsid when using the ICV administration route. No significant differences were observed between the ability of the two capsids to transduce neurons, astrocytes, or oligodendrocytes following IT administrations. In contrast, the IV administration data showed more variation with the AAV9 capsid transducing significantly more neurons, AAV-DJ transducing significantly more astrocytes, and no significant difference observed in the ability of these capsids to transduce oligodendrocytes.

To summarize our findings, we generated a heat map that included a score for each experimental result based on our goal of optimizing transduction of neurological tissue and de-targeting the liver and kidney (Fig. 9). This heat map indicates that overall, the AAV-DJ capsid provides a more desirable outcome regardless of the delivery route used.

Discussion

AAV vectors are being increasingly incorporated into the development of gene therapies for a wide variety of genetically inherited disorders due to their ability to efficiently transduce various cell types, including non-dividing cells with relatively minimal immunogenicity [42–45]. Several naturally occurring and engineered capsids have been evaluated for targeted gene delivery to specific tissues [43, 46, 47]. AAV9 has been found to have broad tropism for a variety of organs and is the gene delivery vehicle used in an FDA-approved therapy for SMA [7] due to its ability to cross the blood brain barrier and efficiently transduce the CNS in children up to two years of age. Despite the overall clinical success with this therapy, there remain challenges due to the tendency of human patients to have high levels of pre-existing antibodies against natural occurring serotypes such as AAV9. Delivery of AAV9 in the presence of high pre-existing antibody levels results in an immune response that attacks the AAV9 and diminishes the therapeutic effect. Therefore, many investigators are working to develop engineered capsids that evade pre-existing neutralizing antibodies or induce milder immune responses, in the hope that this



will allow for more sustained transgene expression and therapeutic benefit at lower doses [48–50].

The AAV-DJ serotype used in our studies was developed and identified through screening pools of hybrid AAV vectors. It was generated from screened combinations of five natural serotypes (AAV 2, 4, 5, 8, and 9) [20]. The screening resulted in an AAV 2/8/9 chimera (AAV-DJ) that differs from its closest AAV serotype relative (AAV2) by 60 amino acids. Several previous studies have shown that AAV-DJ is highly efficient *in vivo* [51–54]. Recently, a non-human primate study demonstrated that AAV-DJ successfully achieved broad transduction throughout the brain [21]. A careful assessment of AAV-DJ transduction as compared to AAV9 in mice was needed to provide a strong rationale for testing this capsid as a gene delivery vehicle to treat neurological disorders in small and large animal models, as well as evaluating its efficacy in future human clinical trials.

AAV-DJ exhibits robust transduction efficiency in both *in vitro* and *in vivo* as compared to several naturally occurring AAV serotypes, including AAV2 and AAV8

[20, 55, 56]. The enhanced transduction profile of AAV-DJ can be attributed to its capsid properties, including altered receptor binding and cellular trafficking mechanisms [20, 23]. Our hypothesis that AAV-DJ would provide more on-target CNS expression and less expression in the liver and kidney turned out to be true, when directly compared to results using the same doses and delivery routes for AAV9 (Fig. 9).

We compared the transduction efficiency of AAV9 and AAV-DJ using three delivery routes (IV, IT, and ICV) to characterize differences and similarities in their abilities to transduce specific regions of the brain, the spinal cord, specific neuronal cell types of interest, and off target organs (liver and kidney). A dose of 1×10^{13} vg/kg was used for IV administrations of these vectors as this aligns well with typical systemic doses used in previous AAV mediated gene therapy studies [31, 57]. A lower dose of 1×10^{12} vg/kg was used for both IT and ICV injections due to volume limitations using these delivery routes [58]. We remained within the typical dose range for each of these delivery routes in mice.

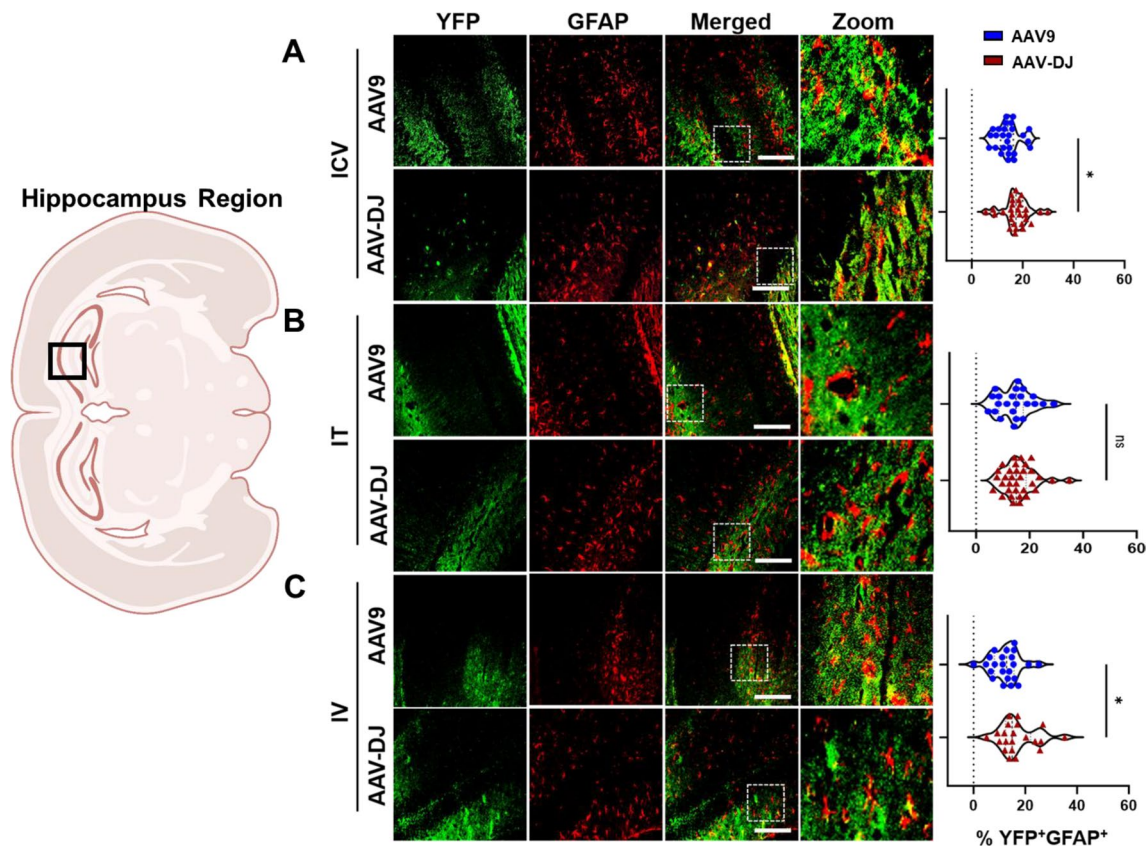


Fig. 8 Relative transduction of neurons between cohorts. YFP transgene expression was compared to an astrocyte cell marker (GFAP) and the co-localization was quantified across cohorts through blinded analysis. Representative immunofluorescence images (from the hippocampus area as indicated in a brain overview image) from each cohort (A) ICV, (B) IT, and (C) IV are provided. For each mouse tissue, five non-overlapping images were acquired from across each of three tissue sections, and evaluated by a trained, blinded observer. The percentages of YFP⁺/GFAP⁺ cells are presented in the right-hand panels. Scale bars = 100 μ m. The white box indicates the zoomed-in portion of the image that is displayed to the right of each row of images

Improved targeting efficiency of neurological gene therapies will help to address the high liver innate and adaptive immune responses that are often observed even in successful AAV gene therapies [26, 59]. Our use of the ubiquitous chicken- β -actin (CBA) promoter to express a luciferase-YFP fusion construct enabled us to noninvasively detect in vivo luciferase activity using IVIS bioluminescence imaging and conduct longitudinal assessments of general transgene expression on live animals [60]. This methodology is easily accessible and simple to perform to gain a broad and general sense of transgene expression through detection of the extent of bioluminescence using a gradient generated from selected regions of interest [61]. This construct also enabled us to perform confirmatory luciferase assays on harvested tissues, and to conduct more precise IF expression analyses of specific cell types using an antibody that recognized YFP on tissue sections.

Although we used a ubiquitous promoter for these studies, promoters do provide another important level of control over vector transgene expression [62]. The use of cell-type specific promoters such as human synapsin

(hSYN) can restrict transgene expression profiles to specific cell types or tissues [63, 64]. Other studies suggest that promoter-capsid interactions can also influence in vivo expression [65, 66]. Future studies designed to pair the AAV-DJ capsid and optimal delivery route with promoter comparisons will further refine CNS targeted AAV-mediated gene therapy strategies.

The mouse strain used can influence the transduction profiles of AAV capsids. One example of this is the AAV-PHP.B family of capsids that requires the Ly6A receptor for efficient transduction and thus, must be used with mice on the C57/BL6 background strain [67]. For this study, we used wild-type FVB/NJ mice and our results were similar to those previously observed in a non-human primate study evaluating neuronal transduction [21]. Thus, as our results are consistent across at least two different species, we are confident that they are not an artifact resulting from the FVB/NJ mouse strain.

One limitation to our study is the duration of these experiments. This study was conducted using a set timeline of nine weeks that is significantly shorter than what would typically be desired in humans where the goal

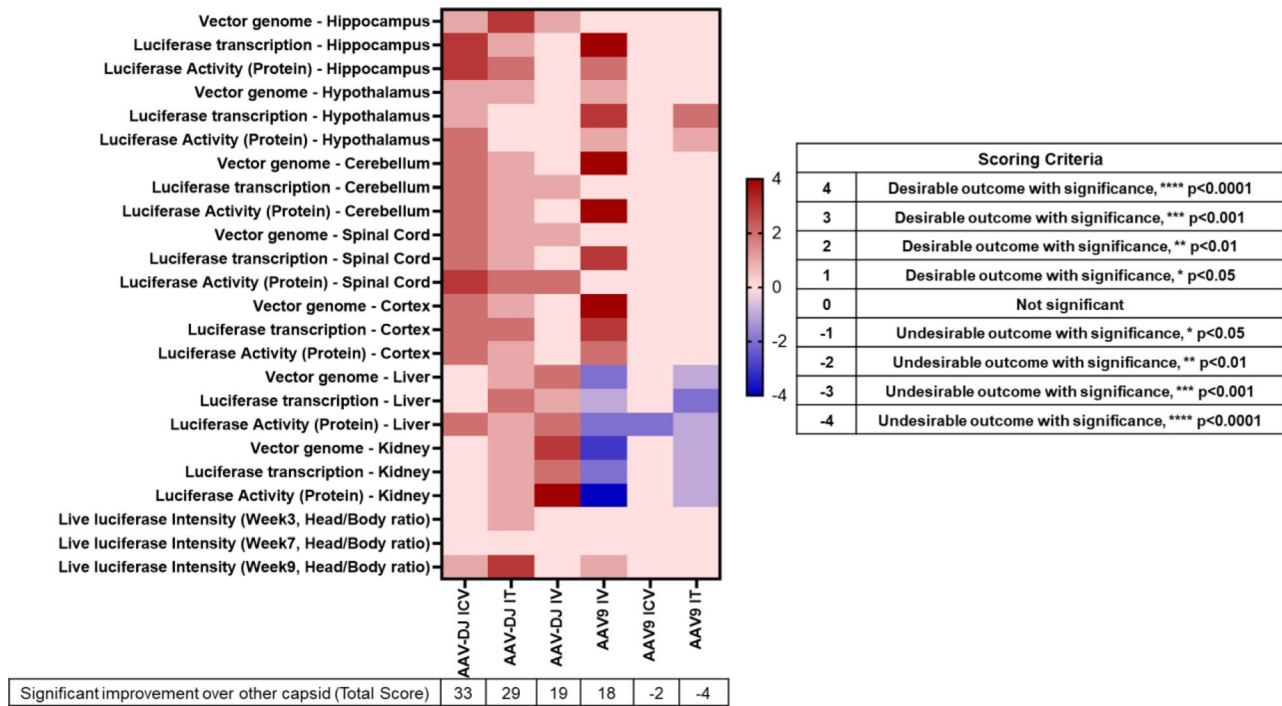


Fig. 9 A heat map summarizing the AAV-mediated gene therapy capsid and delivery route comparison. Scoring criteria are indicated in the right-hand panel based on the statistical significance obtained in each assay as compared to the other capsid

would be to provide therapeutic expression for the lifetime of the patient. While our goal for this study was to establish an optimal AAV capsid and delivery route, other studies will be needed to establish durability of expression based upon these and other factors such as promoter usage and dose. Subsequent studies would also benefit from the use of a large animal model that more accurately represents human neurological tissue size and physiology. Recent developments for gene editing in swine allows for the generation of pig genetic models that more accurately mimic human physiology, anatomy, and lifespan [68]. Swine models more accurately match the size and complexity of the human brain and will be instrumental for the optimization of doses and AAV volumes in the future. Future long-term studies designed to establish the durability of AAV-DJ based or other novel AAV capsids can be performed in swine models to support translation into human clinical trials.

In general, the RNA transcript and protein expression levels we observed were similar to those found in the vg data. Subtle differences are likely related to variances in the distribution of data between cohorts due to factors such as assay sensitivity, post-transcriptional modifications, RNA/protein stability, and translational efficiency [69]. The cumulative data depicted in our heat map show a clear distinction between the two capsids' neurological transduction efficiencies when using the ICV or IT delivery routes. In contrast, cumulative scores between the two capsids following use of the IV delivery route are

similar albeit the capsids demonstrated distinct attributes and limitations. For example, AAV9 (IV) transduces many desirable target organs along with off-target organs (live and kidney) while AAV-DJ profiles are lower in target organs but much lower in off-target organs.

In conclusion, our study indicates that AAV-DJ is superior for targeting the brain and spinal cord while concurrently de-targeting liver and kidney in mice. These findings enable the selection of a combined optimal capsid and administration route for various CNS disease-specific therapeutic targets. This study also establishes a foundation upon which future studies can be designed to test AAV-DJ for use in gene therapies targeting the CNS, evaluate AAV-DJ capsid modifications for improved neuronal transduction, and perform promoter comparisons to further improve the efficacy of gene therapies.

Abbreviations

- AAV Adeno-associated virus
- ANOVA Analysis of Variance
- CBA Chicken β -actin
- cDNA complementary DNA
- CNS Central Nervous System
- FDA Food and Drug Administration
- fLuc Firefly luciferase
- gDNA genomic DNA
- GFAP Glial fibrillary acidic protein (intermediate filament-III)
- HEK293 Human Embryonic Kidney cell line
- ICV Intracerebroventricular
- IF Immunofluorescence
- IP Intraperitoneal
- IT Intrathecal
- ITR Inverted terminal repeats

IV	Intravenous
NeuN	Neuronal specific nuclear protein (Fox-3, Rbfox3, or Hexaribonucleotide Binding Protein-3)
OLIG2	Oligodendrocyte transcription factor 2
PFA	Paraformaldehyde
PBS	Phosphate buffered saline
qPCR	Quantitative Polymerase Chain Reaction
Rep/Cap	Replication and Capsid protein coding
RLUs	Relative Light Units
SEM	Standard error of mean
SMA	SMA (Spinal Muscular Atrophy)
Vg	Vector genome
WT	Wild-type
YFP	Yellow Fluorescent Protein

Supplementary Information

The online version contains supplementary material available at <https://doi.org/10.1186/s12967-024-05599-5>.

Supplementary Material 1

Acknowledgements

This work was supported by the resources and staff at the University of Minnesota University Imaging Centers (UIC: SCR_020997). Thank you to the CFI/ITN Imaging Core and Dr. Jason Mitchell for the microscope training and to Alexia Hang and Frances Sehneah for assistance in RNA and gDNA isolations. Figure 1 was created with the help of BioRender.com.

Author contributions

M.C. and C.A.P. designed the experiments, analyzed the data, and wrote the manuscript with input and editing from P.B.K., G.A., J.A.T., and A.L.D. Virus production, purification and its quality controls were performed by O.F.D. and G.A. AAV administrations and IVIS imaging were performed by M.C., A.L.D. and F.K. M.C. and A.L.D. performed quantitative PCRs and luciferase assays. M.C. and A.L.D. performed histology preparations and M.C. performed immunofluorescence assays. A.L.D., A.H. quantified the immunofluorescence assays blinded. All authors reviewed a draft of the manuscript and provided input.

Funding

This work was supported by the US Food and Drug Administration/Center for Biologics Evaluation and Research, Contract/Grant Number: R01FD007483 (C.A.P. and G.A. MPI), as well as generous support from the Viljem Julijan Association for Children with Rare Diseases.

Declarations

Conflict of interest

Authors declare no conflict of interest.

Received: 17 May 2024 / Accepted: 12 August 2024

Published online: 05 September 2024

References

- Mingozzi F, High KA. Therapeutic in vivo gene transfer for genetic disease using AAV: progress and challenges. *Nat Rev Genet*. 2011;12:341–55.
- Manno CS, Chew AJ, Hutchison S, Larson PJ, Herzog RW, Arruda VR, Tai SJ, Ragni MV, Thompson A, Ozelo M, et al. AAV-mediated factor IX gene transfer to skeletal muscle in patients with severe hemophilia B. *Blood*. 2003;101:2963–72.
- Rangarajan S, Walsh L, Lester W, Perry D, Madan B, Laffan M, Yu H, Vettermann C, Pierce GF, Wong WY, et al. AAV5-Factor VIII gene transfer in severe Hemophilia A. *N Engl J Med*. 2017;377:2519–30.
- Miesbach W, Meijer K, Coppens M, Kampmann P, Klamroth R, Schutgens R, Tangelder M, Castaman G, Schwable J, Bonig H, et al. Gene therapy with adeno-associated virus vector 5-human factor IX in adults with hemophilia B. *Blood*. 2018;131:1022–31.
- George LA, Sullivan SK, Giermasz A, Rasko JEJ, Samelson-Jones BJ, Ducore J, Cuker A, Sullivan LM, Majumdar S, Teitel J, et al. Hemophilia B Gene Therapy with a high-specific-activity factor IX variant. *N Engl J Med*. 2017;377:2215–27.
- Nathwani AC, Tuddenham EG, Rangarajan S, Rosales C, McIntosh J, Linch DC, Chowdhary P, Riddell A, Pie AJ, Harrington C, et al. Adenovirus-associated virus vector-mediated gene transfer in hemophilia B. *N Engl J Med*. 2011;365:2357–65.
- Bevan AK, Duque S, Foust KD, Morales PR, Braun L, Schmelzer L, Chan CM, McCrate M, Chicoine LG, Coley BD, et al. Systemic gene delivery in large species for targeting spinal cord, brain, and peripheral tissues for pediatric disorders. *Mol Ther*. 2011;19:1971–80.
- Smith BK, Collins SW, Conlon TJ, Mah CS, Lawson LA, Martin AD, Fuller DD, Cleaver BD, Clement N, Phillips D, et al. Phase I/II trial of adeno-associated virus-mediated alpha-glucosidase gene therapy to the diaphragm for chronic respiratory failure in pompe disease: initial safety and ventilatory outcomes. *Hum Gene Ther*. 2013;24:630–40.
- Mendell JR, Al-Zaidy SA, Rodino-Klapac LR, Goodspeed K, Gray SJ, Kay CN, Boye SL, Boye SE, George LA, Salabarria S, et al. Current clinical applications of in vivo gene therapy with AAVs. *Mol Ther*. 2021;29:464–88.
- Schnepp BC, Clark KR, Klemanski DL, Pacak CA, Johnson PR. Genetic fate of recombinant adeno-associated virus vector genomes in muscle. *J Virol*. 2003;77:3495–504.
- Clark KR, Sferra TJ, Lo W, Qu G, Chen R, Johnson PR. Gene transfer into the CNS using recombinant adeno-associated virus: analysis of vector DNA forms resulting in sustained expression. *J Drug Target*. 1999;7:269–83.
- Salabarria SM, Corti M, Coleman KE, Wichman MB, Berthry JA, D'Souza P, Tiffet CJ, Herzog RW, Elder ME, Shoemaker LR et al. (2024) Thrombotic microangiopathy following systemic AAV administration is dependent on anti-capsid antibodies. *J Clin Invest*, 134.
- Jayandharan GR, Aslanidi G, Martino AT, Jahn SC, Perrin GQ, Herzog RW, Srivastava A. Activation of the NF-kappaB pathway by adeno-associated virus (AAV) vectors and its implications in immune response and gene therapy. *Proc Natl Acad Sci U S A*. 2011;108:3743–8.
- Rogers GL, Martino AT, Aslanidi GV, Jayandharan GR, Srivastava A, Herzog RW. Innate Immune responses to AAV vectors. *Front Microbiol*. 2011;2:194.
- Ronzitti G, Gross DA, Mingozzi F. Human Immune responses to Adeno-Associated Virus (AAV) vectors. *Front Immunol*. 2020;11:670.
- Fitzpatrick Z, Leborgne C, Barbon E, Masat E, Ronzitti G, van Wittenberghe L, Vignaud A, Collaud F, Charles S, Sola S, M, et al. Influence of pre-existing anti-capsid neutralizing and binding antibodies on AAV Vector Transduction. *Mol Ther Methods Clin Dev*. 2018;9:119–29.
- Prasad S, Dimmock DP, Greenberg B, Walia JS, Sadhu C, Tavakkoli F, Lipshutz GS. Immune responses and immunosuppressive strategies for Adeno-Associated Virus-based gene therapy for treatment of Central Nervous System disorders: current knowledge and approaches. *Hum Gene Ther*. 2022;33:1228–45.
- Sansone VA, Pirola A, Albamonte E, Pane M, Lizio A, D'Amico A, Catteruccia M, Cutrera R, Bruno C, Pedemonte M, et al. Respiratory needs in patients with type 1 spinal muscular atrophy treated with Nusinersen. *J Pediatr*. 2020;219:223–e228224.
- Liguore WA, Domire JS, Button D, Wang Y, Dufour BD, Srinivasan S, McBride JL. AAV-PHPB Administration results in a Differential Pattern of CNS biodistribution in non-human Primates compared with mice. *Mol Ther*. 2019;27:2018–37.
- Grimm D, Lee JS, Wang L, Desai T, Akache B, Storm TA, Kay MA. In vitro and in vivo gene therapy vector evolution via multispecies interbreeding and retargeting of adeno-associated viruses. *J Virol*. 2008;82:5887–911.
- Kondratov O, Kondratova L, Mandel RJ, Coleman K, Savage MA, Gray-Edwards HL, Ness TJ, Rodriguez-Lebron E, Bell RD, Rabinowitz J, et al. A comprehensive study of a 29-capsid AAV library in a non-human primate central nervous system. *Mol Ther*. 2021;29:2806–20.
- Asokan A, Shen S. Redirecting AAV vectors to extrahepatic tissues. *Mol Ther*. 2023;31:3371–5.
- Zincarelli C, Soltys S, Rengo G, Rabinowitz JE. Analysis of AAV serotypes 1–9 mediated gene expression and tropism in mice after systemic injection. *Mol Ther*. 2008;16:1073–80.
- Mendell JR, Al-Zaidy S, Shell R, Arnold WD, Rodino-Klapac LR, Prior TW, Lowes L, Alfano L, Berry K, Church K, et al. Single-dose gene-replacement therapy for spinal muscular atrophy. *N Engl J Med*. 2017;377:1713–22.

25. Yang TY, Braun M, Lembke W, McBlane F, Kamerud J, DeWall S, Tarcsa E, Fang X, Hofer L, Kavita U, et al. Immunogenicity assessment of AAV-based gene therapies: an IQ consortium industry white paper. *Mol Ther Methods Clin Dev.* 2022;26:471–94.
26. Duan D. Lethal immunotoxicity in high-dose systemic AAV therapy. *Mol Ther.* 2023;31:3123–6.
27. Colon-Cortes Y, Hasan MA, Aslanidi G. Intra-tracheal delivery of AAV6 vectors results in sustained transduction in murine lungs without genomic integration. *Gene.* 2020;7635:100037.
28. Krotova K, Aslanidi G. Modifiers of Adeno-Associated virus-mediated gene expression in implication for serotype-universal neutralizing antibody assay. *Hum Gene Ther.* 2020;31:1124–31.
29. Pandya J, Ortiz L, Ling C, Rivers AE, Aslanidi G. Rationally designed capsid and transgene cassette of AAV6 vectors for dendritic cell-based cancer immunotherapy. *Immunol Cell Biol.* 2014;92:116–23.
30. Krotova K, Yoshitomi K, Caine H, C. and, Aslanidi G. Tumor antigen-loaded AAV vaccine drives protective immunity in a melanoma animal model. *Mol Ther Methods Clin Dev.* 2023;28:301–11.
31. Suzuki-Hatano S, Saha M, Rizzo SA, Witko RL, Gosiker BJ, Ramanathan M, Soustek MS, Jones MD, Kang PB, Byrne BJ, et al. AAV-Mediated TAZ gene replacement restores mitochondrial and cardioskeletal function in Barth Syndrome. *Hum Gene Ther.* 2019;30:139–54.
32. Pacak CA, Suzuki-Hatano S, Khadir F, Daugherty AL, Sriramvenugopal M, Gosiker BJ, Kang PB, Cade WT. One episode of low intensity aerobic exercise prior to systemic AAV9 administration augments transgene delivery to the heart and skeletal muscle. *J Transl Med.* 2023;21:748.
33. Hylden JL, Wilcox GL. Intrathecal substance P elicits a caudally-directed biting and scratching behavior in mice. *Brain Res.* 1981;217:212–5.
34. Cheng W, Huang J, Fu XQ, Tian WY, Zeng PM, Li Y, Luo ZG. Intrathecal delivery of AAV-NDNF ameliorates disease progression of ALS mice. *Mol Ther.* 2023;31:3277–89.
35. Smirnov VT, Dubrovskaja FI, Kiseleva TI. (1978) [Action of dimethyldioxane on the generative function of experimental animals]. *Gig Sanit.* 16–8.
36. Hylden JL, Wilcox GL. Intrathecal morphine in mice: a new technique. *Eur J Pharmacol.* 1980;67:313–6.
37. Taylor ZV, Khand B, Porgador A, Monsonego A, Eremenko E. An optimized intracerebroventricular injection of CD4(+) T cells into mice. *STAR Protoc.* 2021;2:100725.
38. Gray SJ, Choi VW, Asokan A, Haberman RA, McCown TJ, Samulski RJ. (2011) Production of recombinant adeno-associated viral vectors and use in vitro and in vivo administration. *Curr Protoc Neurosci.* Chap. 4, Unit 4 17.
39. Jonasson R, Jonsson B, Nordlander R, Oriinius E, Szamosi A. Rate of progression of severity of valvular aortic stenosis. *Acta Med Scand.* 1983;213:51–4.
40. Vulchanova L, Riedl MS, Shuster SJ, Buell G, Surprenant A, North RA, Elde R. Immunohistochemical study of the P2X2 and P2X3 receptor subunits in rat and monkey sensory neurons and their central terminals. *Neuropharmacology.* 1997;36:1229–42.
41. Deverman BE, Pravdo PL, Simpson BP, Kumar SR, Chan KY, Banerjee A, Wu WL, Yang B, Huber N, Pasca SP, et al. Cre-dependent selection yields AAV variants for widespread gene transfer to the adult brain. *Nat Biotechnol.* 2016;34:204–9.
42. Sack BK, Herzog RW. Evading the immune response upon in vivo gene therapy with viral vectors. *Curr Opin Mol Ther.* 2009;11:493–503.
43. Wang D, Tai PWL, Gao G. Adeno-associated virus vector as a platform for gene therapy delivery. *Nat Rev Drug Discov.* 2019;18:358–78.
44. Aguti S, Malerba A, Zhou H. The progress of AAV-mediated gene therapy in neuromuscular disorders. *Expert Opin Biol Ther.* 2018;18:681–93.
45. Ling Q, Herstine JA, Bradbury A, Gray SJ. AAV-based in vivo gene therapy for neurological disorders. *Nat Rev Drug Discov.* 2023;22:789–806.
46. Gao G, Vandenbergh LH, Alvira MR, Lu Y, Calcedo R, Zhou X, Wilson JM. Clades of Adeno-associated viruses are widely disseminated in human tissues. *J Virol.* 2004;78:6381–8.
47. Wang JH, Gessler DJ, Zhan W, Gallagher TL, Gao G. Adeno-associated virus as a delivery vector for gene therapy of human diseases. *Signal Transduct Target Ther.* 2024;9:78.
48. Wang L, Louboutin JP, Bell P, Greig JA, Li Y, Wu D, Wilson JM. Muscle-directed gene therapy for hemophilia B with more efficient and less immunogenic AAV vectors. *J Thromb Haemost.* 2011;9:2009–19.
49. Hareendran S, Balakrishnan B, Sen D, Kumar S, Srivastava A, Jayandharan GR. Adeno-associated virus (AAV) vectors in gene therapy: immune challenges and strategies to circumvent them. *Rev Med Virol.* 2013;23:399–413.
50. Varin J, Morival C, Maillard N, Adjali O, Cronin T. (2021) Risk mitigation of immunogenicity: a Key to Personalized Retinal Gene Therapy. *Int J Mol Sci.* 22.
51. Helfer-Hungerbuehler AK, Shah J, Meili T, Boenzli E, Li P, Hofmann-Lehmann R. (2021) Adeno-Associated Vector-Delivered CRISPR/SaCas9 System reduces Feline Leukemia Virus Production in Vitro. *Viruses.* 13.
52. Wei J, Ran G, Wang X, Jiang N, Liang J, Lin X, Ling C, Zhao B. Gene manipulation in liver ductal organoids by optimized recombinant adeno-associated virus vectors. *J Biol Chem.* 2019;294:14096–104.
53. Holehonnur R, Luong JA, Chaturvedi D, Ho A, Lella SK, Hosek MP, Ploski JE. Adeno-associated viral serotypes produce differing titers and differentially transduce neurons within the rat basal and lateral amygdala. *BMC Neurosci.* 2014;15:28.
54. Jolle C, Deglon N, Pythoud C, Bouzier-Sore AK, Pellerin L. Development of efficient AAV2/DJ-Based viral vectors to selectively Downregulate the expression of neuronal or astrocytic target proteins in the Rat Central Nervous System. *Front Mol Neurosci.* 2019;12:201.
55. Chen X, Wolfe DA, Bindu DS, Zhang M, Taskin N, Goertsen D, Shay TF, Sullivan EE, Huang SF, Kumar R, S., et al. Functional gene delivery to and across brain vasculature of systemic AAVs with endothelial-specific tropism in rodents and broad tropism in primates. *Nat Commun.* 2023;14:3345.
56. Hickey RD, Lillegard JB, Fisher JE, McKenzie TJ, Hofherr SE, Finegold MJ, Nyberg SL, Grompe M. Efficient production of Fah-null heterozygote pigs by chimeric adeno-associated virus-mediated gene knockout and somatic cell nuclear transfer. *Hepatology.* 2011;54:1351–9.
57. Chen X, Wolfe DA, Bindu DS, Zhang M, Taskin N, Goertsen D, Shay TF, Sullivan E, Huang SF, Kumar SR et al. (2023) Functional gene delivery to and across brain vasculature of systemic AAVs with endothelial-specific tropism in rodents and broad tropism in primates. *bioRxiv.*
58. Gong Y, Berenson A, Laheji F, Gao G, Wang D, Ng C, Volak A, Kok R, Kreouzis V, Dijkstra IM, et al. Intrathecal Adeno-Associated viral vector-mediated gene delivery for Adrenomyeloneuropathy. *Hum Gene Ther.* 2019;30:544–55.
59. Ertl HCJ. Immunogenicity and toxicity of AAV gene therapy. *Front Immunol.* 2022;13:975803.
60. Sadikot RT, Blackwell TS. Bioluminescence imaging. *Proc Am Thorac Soc.* 2005;2:537–40.
61. Ezra-Elia R, Obolensky A, Eizenberg A, Ross M, Mintz D, Banin E, Ofri R. Can an in vivo imaging system be used to determine localization and biodistribution of AAV5-mediated gene expression following subretinal and intravitreal delivery in mice? *Exp Eye Res.* 2018;176:227–34.
62. Pacak CA, Sakai Y, Thattaliyath BD, Mah CS, Byrne BJ. Tissue specific promoters improve specificity of AAV9 mediated transgene expression following intravascular gene delivery in neonatal mice. *Genet Vaccines Ther.* 2008;6:13.
63. Chadman KK, Adayev T, Udayan A, Ahmed R, Dai CL, Goodman JH, Meeker H, Dolzhanskaya N, Velinov M. (2023) Efficient delivery of FMR1 across the blood brain barrier using AAVphp construct in adult FMR1 KO mice suggests the feasibility of Gene Therapy for Fragile X Syndrome. *Genes (Basel).* 14.
64. Zheng Y, Xu X, Fan R, Jiang H, Guo Q, Han X, Liu Y, Luo G. Intravitreal Delivery of rAAV2-hSyn-hRS1 results in retinal ganglion cell-specific gene expression and retinal improvement in the R51-KO mouse. *Hum Gene Ther.* 2024;35:342–54.
65. Bohlen MO, McCown TJ, Powell SK, El-Nahal HG, Daw T, Basso MA, Sommer MA, Samulski RJ. Adeno-Associated Virus Capsid-promoter interactions in the Brain Translate from Rat to the Nonhuman Primate. *Hum Gene Ther.* 2020;31:1155–68.
66. Powell SK, Samulski RJ, McCown TJ. AAV capsid-promoter interactions determine CNS cell-selective gene expression in vivo. *Mol Ther.* 2020;28:1373–80.
67. Hordeaux J, Wang Q, Katz N, Buza EL, Bell P, Wilson JM. The Neurotropic properties of AAV-PHPB are limited to C57BL/6J mice. *Mol Ther.* 2018;26:664–8.
68. Perleberg C, Kind A, Schnieke A. (2018) Genetically engineered pigs as models for human disease. *Dis Model Mech.* 11.
69. Liu Y, Beyer A, Aebersold R. On the Dependency of Cellular protein levels on mRNA abundance. *Cell.* 2016;165:535–50.

Publisher's Note

Springer Nature remains neutral with regard to jurisdictional claims in published maps and institutional affiliations.